Ruthenium Carbonyl Clusters in Faujasite Cages: Synthesis and Characterization

Guo-Cheng Shen,*,†,‡ An Ming Liu,§,‡ and Masaru Ichikawa‡

Lash Miller Chemical Laboratories, Department of Chemistry, University of Toronto, 80 St. George Street, Toronto, Ontario, M5S 3H6, Canada, State Key Laboratory of Catalysis, Dalin Institute of Chemical Physics, Chinese Academy of Sciences, Dalin 116023, China, and Catalysis Research Center, Hokkaido University, Sapporo 060, Japan

Received August 7, 1997

The synthesis of the intrafaujasite anchoring of ruthenium carbonyl clusters involves the adsorption of metal carbonyl species or metal ion exchange into faujasite cages followed by reductive carbonylation under an atmosphere of CO and H_2. The characterization of the structure and properties of these samples was based on a multianalytical approach, including FT-IR, UV−vis, PXRD, and EXAFS spectroscopies, CO/H_2 gas chemisorption, and ^{13}CO isotopic exchange. From this study, several key points emerge. (a) $[Ru_3(CO)_{12}]$ clusters thermally diffused into dehydrated faujasite cages. (b) $[Ru_3(CO)_{12}]$ guests in $Na_{56}Y$ were thermally activated, in a hydrogen atmosphere, generating intrafaujasite $[H_4Ru_4(CO)_{12}]$. (c) Hexammineruthenium(III) complexes in $Na_{56}X$ and $Na_{56}Y$ underwent progressive thermal activation, in a CO and H_2 atmosphere. The generation process was considered to occur through conversion of the intermediates $[Ru(NH_3)_5(CO)]^{2+}$ and $Ru^I(CO)_3$ to $[Ru_6(CO)_{18}]^{2-}$. (d) A rapid $^{13}CO/^{12}CO$ isotopic exchange was found to reversibly occur for $[Ru_6(CO)_{18}]^{2-}/Na_{56}X$ under H_2 coexistence. (e) Internal and external confinement of ruthenium carbonyl clusters were compared. (f) Oxidation fragmentation under an O_2 atmosphere and reductive regeneration under a CO and H_2 atmosphere were found to reversibly occur for $[Ru_6(CO)_{18}]^{2-}$ guests. (g) Intrafaujasite anchoring of ruthenium carbonyl clusters showed a strong interaction with the extraframework Na^+ α-cage cations, through involvement of the oxygen end of the bridging or equatorial terminal carbonyl ligands.

Introduction

Organometallics and coordination compounds strategically located and anchored within the cage and channel spaces of different zeolite structure types make possible various applications, such as size/shape-selective catalysis, gas separation/purification, artifical photosynthesis, and electro- and photocatalysis.[1,2] In this regard, higher yields of clusters and a better understanding of the nucleation process of cluster formation and of the resulting chemical properties have been recently developed through organometallic chemistry on surface, gas-phase clusters and novel preparation in faujasite cages.[3,4] The framework structures of some commonly studied faujasites are presented in Figure 1.[5,6] These microporous aluminosilicates are composed of SiO_4 and AlO_4^- tetrahedra joined through shared oxygen bridges. The large cavity in faujasite is typically referred to as the α-cage while the smaller cavities are known as the β-cages and as hexagonal prisms. The net negative charge on the lattice is counterbalanced by exchangeable metal cations (M = Li, Na, K, Rb, or Cs) located at well-defined sites, which

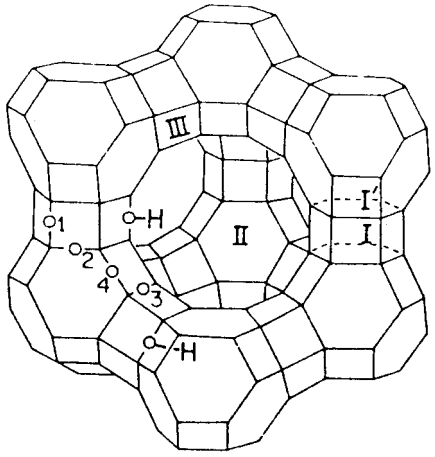

Figure 1. A portion of a Faujasite unit cell, showing framework oxygen numbering and cation and Brönsted acid site designation.

are labeled in Figure 1 according to convention. The oxide framework of faujasite contains Brönsted acid, Lewis acid, and Lewis base sites,[7] which result in what may be thought of as a faujasite that acts as a "solid solvent". This suggests that synthetic chemical routes in organic matrixes can be transferred to gas/solid-state synthetic chemistry inside faujasite cages. Initial studies focused on the production of small clusters within the α or β-cages of faujasite. This involved either the exchange of extraframework Na^+ cage cations into transition metal cations[8] or the insertion/vapor dispersion of organometallic species into

* To whom correspondence should be addressed. E-mail: jshen@yesic.com.
† University of Toronto.
‡ Hokkaido University.
§ Chinese Academy of Sciences.

(1) Ozin, G. A. In *Materials Chemistry*; Interrante, L. V., Casper, L. A., Ellis, A. B., Eds.; American Chemical Society: Washington, DC, 1995; pp 335−371.
(2) Wasowics, T.; Mickalik, J. *Radiat. Phys. Chem.* **1991**, *37*, 427.
(3) Shen, G.-C.; Ichikawa, M. *J. Chem. Soc., Faraday Trans.* **1997**, *93*, 1185.
(4) Shen, G.-C. *J. Am. Chem. Soc.*, submitted.
(5) Breck, D. W. *Zeolite Molecular Sieves*; Wiley: New York, 1974.
(6) Ozin, G. A.; Gil, C. *Chem. Rev.* **1989**, *89*, 1749−1764.
(7) Barthomeuf, D. *Zeolite*: *Science and Technology*; NATO ASI Series, Series E: Applied Sciences 80; Martinus Nijhoff: The Hague, 1984; p 137.

10.1021/ic9709990 CCC: $15.00
Published on Web 09/24/1998

the cages.[9] Intrafaujasite encapsulation of larger organometallic clusters is often achieved through the "ship-in-bottle" technique.[3,4,8,9,10]

This paper focuses on the design and synthesis of ruthenium carbonyl clusters inside faujasite cages, rather than in organic matrixes. A multianalytical approach, including IR, UV−vis, powder X-ray diffraction (PXRD), and extended X-ray absorption fine structure (EXAFS) spectroscopies, CO/H_2 chemisorption, and ^{13}CO isotopic exchange is shown to provide a rather direct and informative picture of the distribution of ruthenium carbonyl clusters among the cavities of faujasite. The mechanism of $Ru^{III}(NH_3)_6$ or $[Ru_3(CO)_{12}]$ reductive carbonylation within the cavities under a CO and H_2 or a H_2 atmosphere and the models of the intrafaujasite anchoring of ruthenium carbonyl clusters, are also discussed.

Experimental Section

I. Sample Preparation. a. Sample a. A faujasite $Na_{56}Y$-supported $[Ru_3(CO)_{12}]$ (3.2 wt % Ru loading or one $Ru_3(CO)_{12}$ per unit cell) sample was prepared by heating a mixture of $Ru_3(CO)_{12}$ (Strem Chemical) with faujasite $Na_{56}Y$ powder (HSZ-320NAA, lot no. D1-9915, Si/Al = 3.0, surface area = 910 $m^2\ g^{-1}$). Faujasite $Na_{56}Y$ powder was dehydrated by evacuation at 623 K for 2 h and then mixed mechanically with $[Ru_3(CO)_{12}]$ under an N_2 atmosphere at 300 K. This phase showed PXRD reflections at 2θ = 12.3, 12.6, 16.1, 25.9, and 30.0, ascribed to $[Ru_3(CO)_{12}]$, as well as peaks for the $Na_{56}Y$. After 48 h of heating at 333 K, the PXRD reflections for $[Ru_3(CO)_{12}]$ completely disappeared, leaving only the PXRD peaks for $Na_{56}Y$. The resulting light yellow sample was denoted sample a and was characterized by FT-IR and UV−vis spctroscopies.

b. Sample b. A partial pressure of H_2 (400 Torr) was introduced into sample a, which did not produce any significant effect or color change at room temperature, even after 100 h. However, when the temperature was raised to 363 K, a relevant vaporization immediately occurred. After 24 h under an H_2 atmosphere, the IR and diffuse reflectance spectra identified bands of the yellow sublimate, which is denoted sample b (3.2 wt % Ru loading).

c. Samples c and d. $[Ru(NH_3)_6]^{3+}$-exchanged $Na_{56}X$ ($[Ru(NH_3)_6]^{3+}/Na_{56}X$, 3.2 wt % Ru) and $[Ru(NH_3)_6]^{3+}$-exchanged $Na_{56}Y$ ($[Ru(NH_3)_6]^{3+}/Na_{56}Y$, 3.2 wt % Ru) were respectively prepared by slow addition of an aqueous solution of $Ru(NH_3)_6Cl_3$ (Strem Chemical Co.) to a $Na_{56}X$ slurry (Union Shown K.K. 13X, lot no. 9380113, Si/Al = 1.6, surface area = 870 $m^2\ g^{-1}$) or to a $Na_{56}Y$ slurry (HZS-320NAA, lot no. D-9915, Si/Al = 3.0, surface area = 910 $m^2\ g^{-1}$) with rapid stirring for 3 h. The ion exchange was continuously performed for another 48 h at room temperature (rt). This was then filtered, washed free of Cl^{-1} ions with deionized H_2O, and dried in air at rt.

The IR wafer of $[Ru(NH_3)_6]^{3+}/Na_{56}X$ was exposed to 200 Torr of CO and 200 Torr of H_2 in a closed circulation system and heated from 298 to 393 K. After 22 h, the carbonylated sample changed apparent color from red to pale yellow. The resulting sample is denoted sample c. The IR and UV−vis spectra were recorded during the generation process of sample c.

The IR wafer of $[Ru(NH_3)_6]^{3+}/Na_{56}Y$ was exposed to 200 Torr of CO and 200 Torr of H_2 in a closed circulation system and heated from 300 to 413 K. After 48 h, the resulting sample changed apparent color from red to lemon yellow and showed the IR carbonyl vibration frequencies. This product is denoted sample d.

d. Sample e. SiO_2 (Aerosil 200 Degussa), with a nominal surface area of 200 $m^2\ g^{-1}$, was dried by heating to 623 K for 4 h in a vacuum and then was added to a solution of $[Ru(NH_3)_6]^{3+}Cl_3$ in dichloromethane (CH_2Cl_2) with rapid stirring for 6 h. After the reaction was complete the solvent was removed through evacuation, followed by drying in air at rt. The IR wafer of $[Ru(NH_3)_6]^{3+}/SiO_2$ was exposed to a CO and H_2 atmosphere in a closed circulation system with the same temperature-programmed heating as that used for sample c. The resulting IR wafer showed the stable IR carbonyl stretching frequencies. This product is denoted sample e.

The concentration of Ru in samples a−e was determined using an inductively coupled plasma (ICP) atomic emission spectrometer. Attempts to extract organometallic species from samples a and b were carried out through hexane solution and from samples c and d they were carried out through dichloromethane solution.

II. Characterization of Samples. a. IR Spectroscopy. In situ IR spectra of the samples were recorded with a Shimadzu FT-IR 4200 double-beam spectrometer with 20−100 co-added scans at 2 cm^{-1} resolution. The sample was pressed into a self-supporting wafer (8 mg cm^{-2}) in an N_2 atmosphere box and mounted in a quartz IR cell with CaF_2 windows connected to a Pyrex glass line (10^{-5} Torr) vacuum closed circulating. The IR cell was equipped with an electric heater and a liquid N_2 reservoir for high- and low-temperature measurements. The contribution of the gas phase was compensated by using a reference IR cell having the same optical length as the sample cell. ^{13}CO isotopic exchange reactions were performed in the IR cell using enriched ^{13}CO (98%) purchased from Merck Reagent Co. Ltd. Before use, all gases were passed through traps to remove water and/or oxygen.

b. EXAFS Spectroscopy. EXAFS measurements were carried out at the Photon Factory in Japan National Laboratory for High Energy Physics (KEF-PF) using synchrotron radiation with an electron energy of 2.5 GeV at currents of 80−150 mA. The amount of sample in a wafer was calculated at the Ru K absorption edge, and the sample wafers were stored in specially designed Pyrex glass cells with Kapton film windows (50 nm thick). The spectra at the Ru K edge were measured at 296 K under vacuum using a Si(111) double crystal monochromator. The reference samples used were crystalline $[PPN]_2[Ru_6(CO)_{18}]$ and Ru foil.

c. EXAFS Data Analysis. The EXAFS data were extracted from the measured absorption spectra by standard methods.[11,12] The normalization was done by dividing the absorption intensities by the height of the absorption edge and subtracting the background using cubic spline routines. The final EXAFS function was obtained by averaging the individual background-subtracted and normalized EXAFS data (two scans for each sample). The main contributions to the spectra were isolated by inverse Fourier transformation of the final EXAFS function over a selected range in *R*-space. The analysis was performed on these Fourier-filtered data using empirical parameters (the phase shift and backscattering amplitude functions) obtained from reference samples. The parameters characterizing high-*Z* (Ru) and low-*Z* (C, O) contributions were reliably determined by multiple-shell fitting in *k* space (*k* is the wave vector) and *R* space (*R* is the distance from the absorbing atom) with application of K^3 weighting of the Fourier transform. The accuracy on the parameters was estimated as $0.02 < \sigma < 0.08$ and $-10 < \Delta E° < 10$. The residual factor $= \int |k^3\chi^{obs}(k) - k^3\chi^{calc}(k)|^2\, dk / \int |k^3\chi^{obs}(k)|^2\, dk$ was less than 15% for optimized coordination numbers and bond lengths.[12]

d. Powder X-ray Diffraction (PXRD) and Diffuse Reflectance. The PXRD measurement was carried out using a MAC Science diffractometer with Cu Kα radiation [λ = 1.5418 Å]. Diffuse reflectance spectra were recorded on a Shimadzu UV-2200 series spectrometer with a photomultiplier detector. $BaSO_4$ was used as a reference. The samples were stored in U-type Pyrex glass cells with Heraeus Amersil quartz windows for measurement of evacuation and adsorption.

Results

I. Characterization of Sample a. Sample a is a light yellow $Na_{56}Y$-supported ruthenium carbonyl species. The IR spectrum in Figure 2A, trace 2, and Table 1 shows ν_{co} bands at 2122w, 2067s, and 2025s cm^{-1} and is identified as $[Ru_3(CO)_{12}]$, from the resemblance of the IR bands to those of crystalline $[Ru_3$-

(8) Rao, L.-F.; Fukuoka, A.; Kosugi, N.; Kuroda, H.; Ichikawa, M. *J. Phys. Chem.* **1990**, *94*, 5317.
(9) Shen, G.-C.; Shido, T.; Ichikawa, M. *J. Phys. Chem.* **1996**, *100*, 16947.
(10) Lunsford, J. H. *ACS Symp. Ser.* **1977**, *40*, 473.
(11) van Zon, J. B. A. D.; Koningsberger, D. C.; van't Blik, H. F. J.; Sayers, D. E. *J. Chem. Phys.* **1985**, *12*, 5742.
(12) Kosugi, N.; Kuroda, H. *Program EXAFS 2*; Research Center for Spectrochemistry: University of Tokyo, 1988.

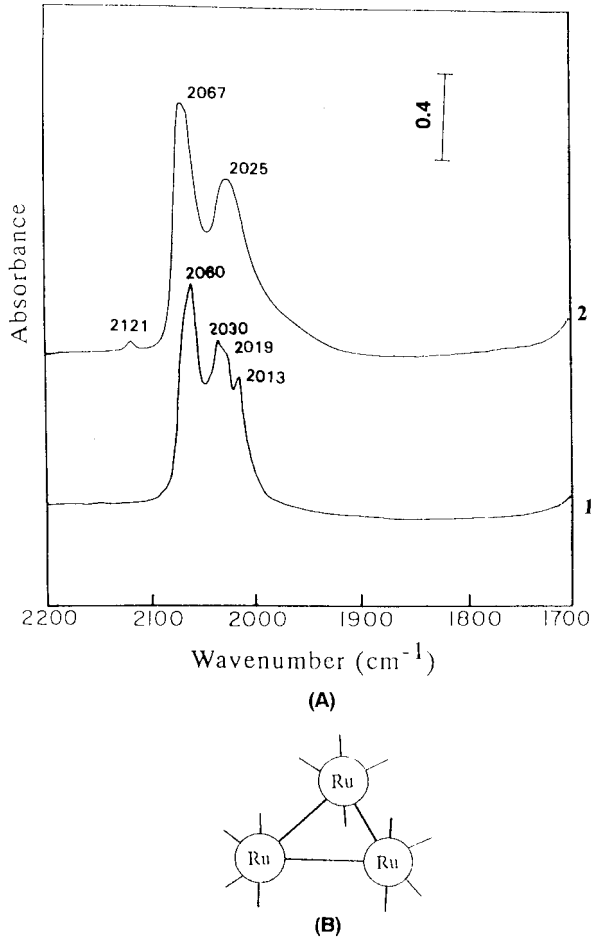

Figure 2. (A) FT-IR spectra obtained for (trace 1), crystalline $[Ru_3(CO)_{12}]$ in hexane solution and (trace 2), sample a. (B) Molecular configuration of crystalline $[Ru_3(CO)_{12}]$.

Table 1. Carbonyl Stretching Frequencies and Assignment for $[Ru_3(CO)_{12}]$ and $[Ru_3(CO)_{12}]/Na_{56}Y$

		ν_{co}/cm^{-1}	
assignment	activity	$[Ru_3(CO)_{12}]^a$	$[Ru_3(CO)_{12}]/Na_{56}Y$
$\nu_1(A_1')$	Raman	2120	
$\nu_5(E')$	IR, Raman	2060	2067
$\nu_5(E')$	IR, Raman		2122
$\nu_2(A_1')$	Raman	2036	
$\nu_4(A_2'')$	IR	2030	2025
$\nu_6(E')$	IR, Raman	2019	
$\nu_7(E')$	IR, Raman	2013	
$\nu_3(A_2')$		2000	
$\nu_8(E'')$	Raman	1995	

[a] Reference 27.

$(CO)_{12}]$ in hexane solution (2060vs, 2030s, 2019sh, and 2013m)[13] (Figure 2A, trace 1). This suggests that $[Ru_3(CO)_{12}]$ is highly dispersed in the cavities of $Na_{56}Y$. The diffuse reflectance spectrum of sample a shows the absorption bands at 400 and 328 nm (Table 2), closely resembling those of crystalline $[Ru_3(CO)_{12}]$ (Table 2: $\lambda_{max} = 392$ nm, $\sigma-\sigma^*$ transition of Ru−Ru; $\lambda_{sh} = 320$ nm, $\sigma^{*\prime}-\sigma^*$ transition of Ru−Ru).[14]

II. Characterization of Sample b. The IR bands of sample b at 2085s, 2070vs, 2031s, 2008m, and 1992w cm^{-1} (Figure 3,

Table 2. Electronic Absorption Band Maxima of Ruthenium Carbonyl Cluster: Dependence on Metal−Metal Bond Strength

sample	λ_{max}/nm	assignment
$[Ru_3(CO)_{12}]^a$	390	$\sigma \rightarrow \sigma^*$
	320	$\sigma^{*\prime} \rightarrow \sigma^*$
sample a	400	$\sigma \rightarrow \sigma^*$
	328	$\sigma^{*\prime} \rightarrow \sigma^*$
$[H_4Ru_4(CO)_{12}]^b$	360	$\sigma^{*\prime} \rightarrow \sigma^*$
sample b	364	$\sigma^{*\prime} \rightarrow \sigma^*$
$[PPN]_2[Ru_6(CO)_{18}]$	285	
	235	
$[Ru_6(CO)_{18}]/Na_{56}X$	287	
	235	

[a] References 14 and 25. [b] Reference 15.

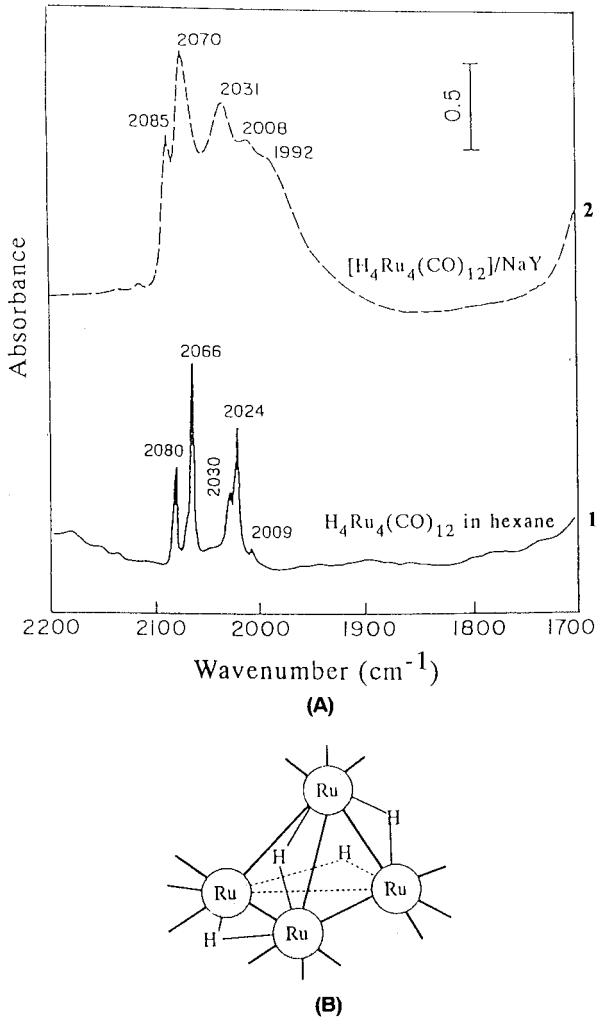

Figure 3. (A) FT-IR spectra obtained for (trace 1), crystalline $[H_4Ru_4(CO)_{12}]$ in hexane solution and (trace 2), sample b. (B) Molecular configuration of crystalline $[H_4Ru_4(CO)_{12}]$.

trace 2) closely resemble those of $[Ru_4H_4(CO)_{12}]$ in hexane with bands of 2080s, 2066vs, 2030m, 2024s, and 2009w cm^{-1} (Figure 3A, trace 1, and Table 3).[15] Table 2 lists the diffuse reflectance absorption of the yellow sample b at 364 nm, which is practically identical to that observed for the yellow crystal $[H_4Ru_4(CO)_{12}]$ ($\lambda_{max} = 360$ nm assigned to $\sigma^{*\prime}-\sigma^*$ transition of Ru − Ru).[15]

III. IR Characterization of the Generation Process for Samples c and d. A fresh sample of $[Ru(NH_3)_6]^{3+}/Na_{56}X$ shows IR bands at 1640 and 1356 cm^{-1} (Figure 4A, trace 1),

(13) (a) Dossi, C.; Psaro, R.; Roberto, D.; Ugo, R.; Zanderighi, G. *Inorg. Chem.* **1990**, *29*, 4368. (b) Knox, S. A. R.; Koepke, J. W.; Andrews, M. A.; Kaesz, H. D. *J. Am. Chem. Soc.* **1975**, *97*, 3942.

(14) Yawney, D. B. W.; Stone, F. G. A. *J. Chem. Soc. A* **1969**, 502.

(15) Geoffroy, G. L.; Gladfelter, W. L. *J. Am. Chem. Soc.* **1977**, *99*, 7565.

Table 3. Carbonyl Stretching Frequencies for Crystalline $[H_4Ru_4(CO)_{12}]$ and $[H_4Ru_4(CO)_{12}]/Na_{56}Y$

ν_{co}/cm^{-1}		
$[H_4Ru_4(CO)_{12}]$		$[H_4Ru_4(CO)_{12}/Na_{56}Y$
IR	Raman[a]	IR
	2019 (s)	
2080 (s)	2078 (w)	2085 (s)
2066 (vs)	2061 (w)	2070 (vs)
2030 (m)	2030 (m)	2031 (s)
2024 (s)	2021 (s)	2008 (m)
2009 (w)	2014 (s)	1992 (w)
	2010 (s)	
	2002 (m)	
	1990 (m)	
	1585 (w)	
	1290 (w)	

[a] Reference 13b.

which are attributed to ν_2, δ(H−N−H), and ν_4, δ(H−N−H), of the ammonia ligand, respectively.[16] On exposing an IR wafer of the fresh sample to CO + H_2 (200 Torr + 200 Torr) in a closed circulating system at 353 K, IR bands arose at 2072w, 2000w, and 1939m cm^{-1} (Figure 4A, trace 2), with the latter predominant band assigned to the $[Ru(NH_3)_5(CO)]^{2+}$ species. Simultaneously, the original band at 1356 cm^{-1} shifts to 1331 cm^{-1} with a decrease in intensity and a new band appears at 1468 cm^{-1}, attributed to ν_4, δ(N−H) of NH_4^+. When the temperature was raised to 393 K, the IR spectrum showed peaks at 2088, 2048, 2014, and 1952 cm^{-1} (Figure 4A, trace 3). The bands at 2088 and 2014 and 2048 and 1952 cm^{-1} can be ascribed to the $Ru^I(CO)_2$ and $Ru^I(CO)_3$ species, respectively.[17] In addition to carbonyl bands, an unidentified peak emerges at low wavenumbers (862 cm^{-1}), probably associated with the interaction of the mononuclear ruthenium carbonyl species with the oxygen of the faujasite framework.[18,19] After 22 h at 393 K, a steady-state spectrum (Figure 4A, trace 4) is observed, exhibiting carbonyl bands at 2000s, 1970vs, 1925m, and 1747w cm^{-1}, while the band at 862 cm^{-1} disappeared. The resultant bands of sample c closely resemble those of $[N(PPh_3)_2]_2[Ru_6(CO)_{18}]$ in dichloromethane [ν_{co}: 2006s, 1986vs, 1930m and 1754w cm^{-1}][20] (Figure 4 parts B and C) but with shifting of the carbonyl band to lower frequency.

In another series of experiments, the $[Ru(NH_3)_6]^{3+}/Na_{56}X$ was carbonylated only in the presence of CO with the same temperature-programmed heating as that described for sample c. Two doublet IR bands at 2087 and 2016 and 2048 and 1950 cm^{-1} indicated the synthesis of $Ru^I(CO)_2$ and $Ru^I(CO)_3$ species and that $[Ru_6(CO)_{18}]^{2-}$ was not formed in $Na_{56}X$. The results are therefore consistent with the proposition that hydrogen gas induced the coalescence of Ru and facilitated the synthesis of $[Ru_6(CO)_{18}]^{2-}$ inside $Na_{56}X$ cages.

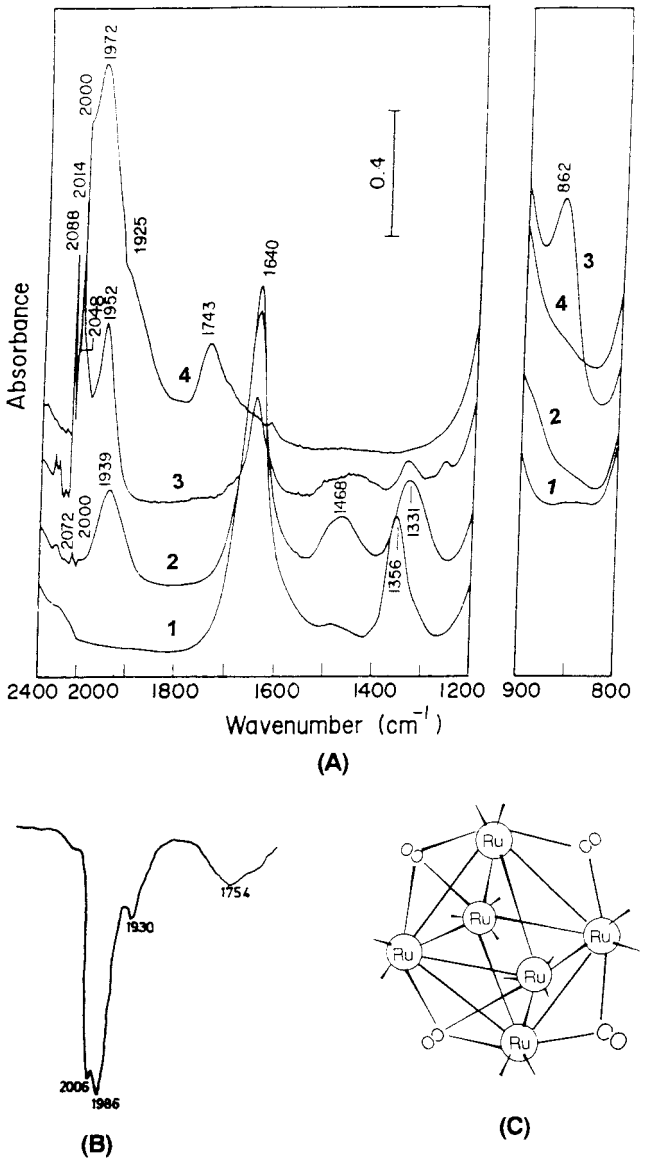

Figure 4. (A) In situ FT-IR spectra in the reaction of $[Ru(NH_3)_6]^3$- with CO and H_2 (200 and 200 Torr) at 298−393 K: (trace 1) initial spectrum in vacuo, 298 K; (trace 2), 353 K; (trace 3), 393 K, 30 min; (trace 4), sample c, 393 K, 22 h. (B) FT- IR spectrum obtained for crystalline $[Ru_6(CO)_{18}]^{2-}$ in dichloromethane solution. (C). Molecular configuration of crystalline $[Ru_6(CO)_{18}]^{2-}$.

When an IR wafer of $[Ru^{III}(NH_3)_6]/Na_{56}Y$ was exposed to a CO and H_2 atmosphere at rt it did not produce any significant effect or color change. However, when the temperature was raised to 413 K, a relevant reaction immediately occurred. The final IR spectrum of sample d shows bands at 2054vs and 1937w cm^{-1} (Table 4) closely resembling those of $[HRu_6(CO)_{18}]^-$ in CH_2Cl_2 solution (ν_{co}: 2027vs and 1957w cm^{-1})[20] with the exception of the shift of carbonyl bands being consistent with well-known ion-pairing effects.[21]

IV. Diffuse Reflectance Characterization of the Generation Process for Sample c. Figure 5 shows the in situ reflectance spectra of the reaction of $[Ru(NH_3)_6]^{3+}/Na_{56}Y$ under an atmosphere of CO of 200 Torr and H_2 of 200 Torr. The parent sample shows four absorption bands at 285, 380, 555, and 750 nm (Figure 5, trace 1). The 555 nm band is close to Ru-red.[22] The band distribution caused by the hexaamine

(16) Nakamoto, K. *Infrared and Raman Spectra of Inorganic and Coordination Compounds*, 3rd ed.; Wiley: New York, 1978; p 199.
(17) (a) Shen, G.-C.; Ichikawa, M. *J. Phys. Chem.* **1996**, *100*, 14265. (b)-Verdonck, J. J.; Schoonheydt, R. A.; Jacobs, P. A. *J. Phys. Chem.* **1983**, *87*, 683.
(18) Ozkar, S.; Ozin, G. A.; Moller, K.; Bein, T. *J. Am. Chem. Soc.* **1990**, *112*, 9575.
(19) (a) Kurodo, Y.; Kotani, A.; Maeda, H.; Moriwaki, H.; Morimoto, T.; Nagao, M. *J. Chem. Soc., Faraday Trans.* **1992**, 1583. (b) Li, C.; Domen, K.; Maruya, K.; Onishi, T. *J. Am. Chem. Soc.* **1989**, *111*, 7683.
(20) (a) Eady, C. R.; Johnson, B. F. G.; Lewis, J.; Malatesta, M. C. *J. Chem. Soc., Chem. Comm.* **1976**, 945. (b) Eady, C. R.; Jackson, P. F.; Johnson, B. F. G.; Lews, J.; Malatesta, M. C. *J. Chem. Soc., Dalton Trans.* **1980**, 383. (c) Hayward, C. M. T.; Shapley, J. *Inorg. Chem.* **1982**, *21*, 3816.
(21) Schmidt, R.; Amiridis, M. D.; Dumesic, J. A.; Zelewski, L. M.; Millman, W. S. *J. Phys. Chem.* **1992**, *96*, 1407.

Table 4. Carbonyl Stretching Frequencies and Assignment for $[Ru_6(CO)_{18}]^{2-}$, $[Ru_6(CO)_{18}]^{2-}/Na_{56}X$, $Ru^I(CO)_2/Na_{56}X$, $Ru^I(CO)_3/Na_{56}X$, $[HRu_6(CO)_{18}]^-$, and $[HRu_6(CO)_{18}]^-/Na_{56}Y$

IR ν_{co}/cm^{-1}					
$[Ru_6(CO)_{18}]^{2-}$ [a]	$[Ru_6(CO)_{18}]^{2-}$/NaX	$Ru^I(CO)_2$/NaX	$Ru_3^I(CO)_3$/NaX	$[HRu_6(CO)_{18}]^-$ [a]	$[HRu_6(CO)_{18}]^-$/NaY
2006 (s)	2000 (s)	2088 (s)	2048 (s)	2027 (vs)	2054 (vs)
1986 (vs)	1972 (vs)	2014 (m)	1952 (m)	1957 (w)	1937 (w)
1930 (m)	1925 (m)				
1754 (w)	1747 (w)				

[b] Reference 21.

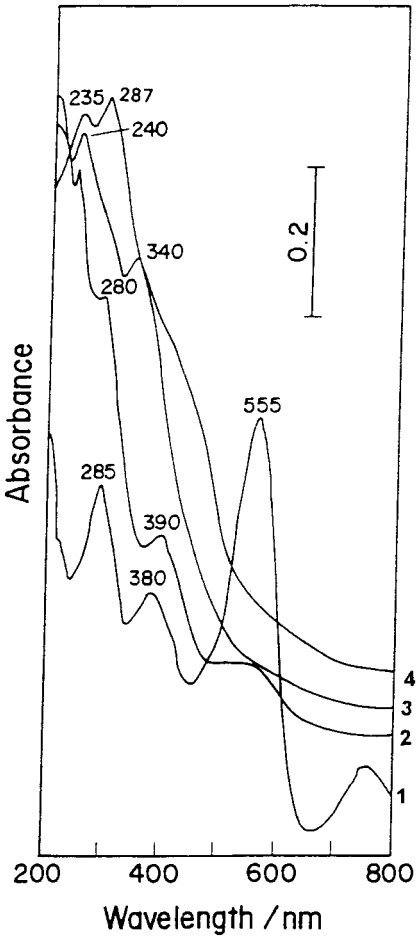

Figure 5. In situ diffuse reflectance in the reaction of $[Ru(NH_3)_6]^{3+}/Na_{56}X$ with CO and H_2 (200 and 200 Torr) at 298−393 K: (trace 1) initial spectrum in vacuo, 298 K, (trace 2), 343 K, 20 h; (trace 3) 373 K, 20 h; (trace 4), sample c, 393 K, 22 h.

ligands is unstable in $Na_{56}X$ and is easily converted to Ru-red or Ru-brown, having a wine-red color.[17b] After 20 h at 343 K under a CO and H_2 atomosphere, the diffuse reflectance spectrum is transformed into an absorption curve with bands at 235, 280, 390, and 550 nm (Figure 5, trace 2) and the sample appears light yellow. As the temperature reached 373 K for 46 h, two new absorption bands at 240 and 340 nm are observed (Figure 5, trace 3). Unfortunately, it is difficult to assign in detail these two bands at present. However, in comparison with the IR spectrum of the relative sample, such bands are associated with the formation of mononuclear ruthenium carbonyl species in $Na_{56}X$. After the sample was heated for 22 h at 393 K, new bands emerged at 235 and 287 nm (Figure 5, trace 4). The reflectance spectrum of the resulting sample c at 235 and 287 nm closely resembles those of crystalline $[PPN]_2[Ru_6(CO)_{18}]$ in tetrahydrofuran (THF) solution (λ_{max} = 235 and 285 nm in Table 2).

When the organometallic species was extracted from the synthetic samples a and b by hexane and from samples c and d by CH_2Cl_2 solution, the supernatant solution remained colorless and showed no IR absorption in the CO stretching region. Further, no appreciable CO frequency shifts were observed when $[Ru_3(CO)_{12}]$, $[H_4Ru_4(CO)_{12}]$, $[Ru_6(CO)_{18}]^{2-}$, or $[HRu_6(CO)_{18}]^-$ was deposited from the organic solution onto the faujasite wafer. Chemical composition of the samples was determined by elemental inductively coupled plasma (ICP), which showed that within experimental error, Ru wt % is ca. 3.2%, corresponding to the concentration of Ru in the initial preparation.

V. EXAFS Data Characterization of Sample c. To obtain more insight into the structure of the intrafaujasite anchoring of ruthenium carbonyl dianionic clusters and especially into the metal framework, the EXAFS spectra of the Ru *K*-edge of sample c was analyzed by a curve-fitting method on the basis of the multiple-scattering theory.[23] The EXAFS function was obtained from the average X-ray absorption spectra by a cubic spline background subtraction and were then normalized by division by the height of the absorption edge. The raw EXAFS data characterizing sample c (Figure 6i) shows oscillations up to a value of *K*, the wave vector, of about 15 $Å^{-1}$ clearly indicating the presence of near-neighbor high atomic weight backscatterers, which are inferred to be Ru atoms. The Fourier transform (Figure 6ii) was obtained from the raw EXAFS data with a K^3-weighting in the range $3.1 < K/Å^{-1} < 15$. The Fourier transformed data were then inverse transformed in the range 1−3.2 Å to *R* space for isolation of the major contributions from low-frequency noise and high-shell contribution. Since the IR data indicated that carbonyl ligands were also present in sample c, the peak in the range $1.0 < R/Å < 3.2$ is attributable to the three shell of Ru−Ru, Ru−C, and Ru(−C−)O contributions. Since the Ru(−C−)O contribution was found to be strongly coupled with the Ru−Ru contribution, these two contributions had to be analyzed simultaneously. The structural parameters were estimated initially by fitting the data in the high-*K* range ($8.5 < K/Å^{-1} < 15$). The multiple scattering associated with the Ru(−C−)O group was found to be significant, with the Ru−C contribution being insignficant in this range. Further analysis, following subtraction of the calculated Ru−Ru and Ru(−C−)O contributions from the raw data, led to characterization of the Ru−C contribution. The fit of the raw data with the sum of the three contributions was still not satisfactory, and it was inferred that another contribution had to be accounted for. A fourth contribution involved another low atomic number backscatterer, which was assumed to be the oxygen of faujasite, referred to as Ru−Oz. The initial structural parameters characterizing the Ru−C and Ru−Oz contributions were obtained by fitting the residual spectrum. The Ru−Ru, Ru−C, Ru(−C−)O, and Ru−Oz contributions

(22) (a) Earley, J. E.; Fealey, T. *J. Chem. Soc., Chem. Comm*. **1971**, 331. (b) Stanko, J. A.; Stanishak, T. W. *Inorg. Chem*. **1969**, *8*, 2156.

(23) (a) Teo, B. K. *J. Am. Chem. Soc*. **1981**, *103*, 3390. (b) Teo, B. K. *EXAFS: Basic Principles and Data Analysis*; Springer: Berlin, 1986.

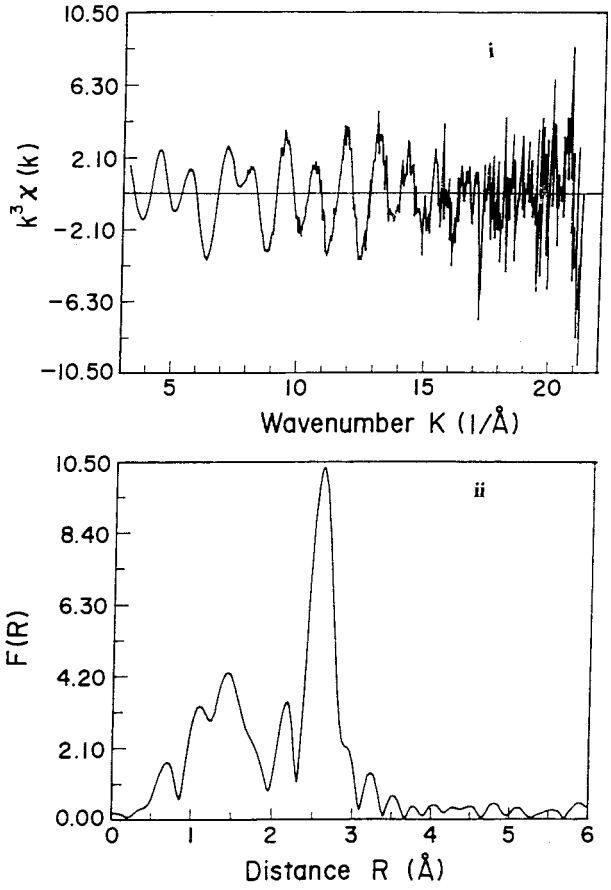

Figure 6. Ru K-edge EXAFS data for synthetic sample c: (i) K^3-weighted EXAFS spectrum $K^3\chi(k)$ vs K; (ii) Fourier transform of K^3-weighted EXAFS spectrum $K^3\chi(k)$ vs R.

Table 5. Results of the Curve-Fitting Analysis of Ru K-edge EXAFS Data Obtained at 296 K for Sample c[a]

shell	CN	R/Å	$\Delta E°$/eV	σ/Å
Ru−Ru	3.5	2.82	12.85	0.067
Ru−O	3.0	3.01	−5.63	0.052
Ru−O	3.1	1.86	−6.67	0.060
Ru−Oz (zeolite)	0.3	2.26	3.66	0.085

[a] Notation: CN, coordination number for absorber−backscatterer pair; R, radial absorber−backscatterer distance; σ, Debye−Waller factor; $\Delta E°$, inner potential correction (correction of the edge position).

were then determined simultaneously by adjusting the coordination parameters based on the initial estimated value. The interaction was continued until good overall agreement was obtained. The results of curve-fitting analyses with the best calculated coordination parameters are shown in Table 5. The data indicate a Ru−Ru coordination number of 3.5 with an average distance of 2.82 Å, a Ru−C coordination number of 3.1 at an average distance of 1.86 Å, a Ru(−C−)O coordination number of 3.0 at an average distance of 3.01 Å, and a Ru−Oz coordination number of 0.3 at an average distance of 2.26 Å. The average Ru−Ru coordination number of 3.5 suggests a cluster containing four to six Ru atoms, while the Ru−Ru distance of 2.82 Å is nearly the same as the value found in $[N(PPh_3)]_2[Ru_6(CO)_{18}]$ in the crystalline state (2.80−2.89 Å).[24] Since the coordination number for crystalline $[Ru_6(CO)_{18}]^{2-}$ is 4, it can be deduced that about 87% of the Ru atoms of sample c are present as an $[Ru_6(CO)_{18}]^{2-}$ cluster, based on the ratio of 3.5:4. The contribution of Ru−Oz indicates that in addition to $[Ru_6(CO)_{18}]^{2-}$ there are other Ru species formed that are bonded to the framework of faujasite via oxygen. A reasonable explanation is that the minor species present, along with the dianionic clusters, are mononuclear carbonyl species, which results in a Ru−Ru coordination number of <4.

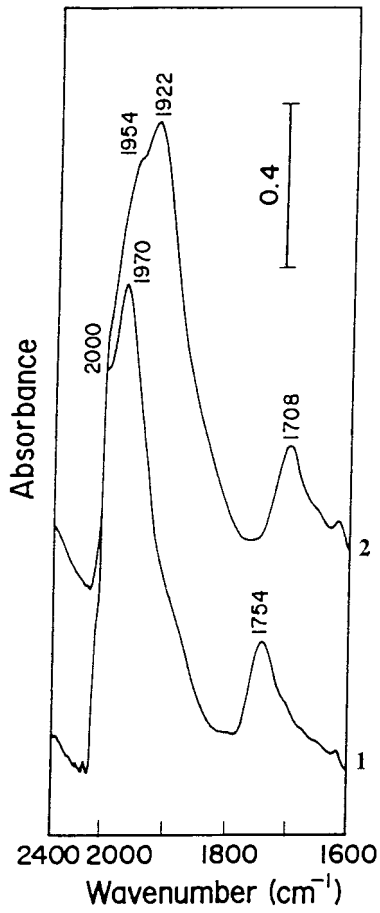

Figure 7. In situ FT-IR spectra obtained for (trace 1), sample c in vacuo and (trace 2) ^{13}CO isotopic exchange of sample c under ^{13}CO and H_2 (20 and 20 Torr) atmosphere at 353 K for 2 h.

On the basis of IR, UV−vis, and EXAFS spectroscopies, one can safely say that the dianionic ruthenium carbonyl clusters were synthesized in $Na_{56}X$.

VI. ^{13}CO Exchange Reaction and Reversible Regeneration of Sample c. On exposure of sample c to ^{13}CO of 20 Torr and H_2 of 20 Torr at 353 K for 2 h, the bands of terminal CO at 2000 and 1970 cm^{-1} and bridging CO at 1754 cm^{-1} were completely replaced by new bands at 1954, 1922, and 1708 cm^{-1}, respectively (Figure 7, trace 2). The values of the band shifts after isotopic exchange were between 44 and 48 cm^{-1}, roughly in the range calculated according to the two-atom model ($\Delta\nu = 39-44$ cm^{-1}). Furthermore, this process was reversible when normal CO and H_2 were introduced under same conditions. These results suggest there is no change in the metal skeleton of sample c during isotopic exchange. However, in the absence of hydrogen, isotopic exchange does not proceed and sample c is unstable upon exposure to CO alone, even at 323 K.

The structure of $[Ru_6(CO)_{18}]^{2-}$ in the cages is very sensitive to oxygen. When the wafer of sample c in the IR cell was brought in contact with 100 Torr of O_2 at rt, the bridging CO band at 1754 cm^{-1} quickly disappeared. On raising the temperature to 403 K, a new spectrum was obtained, showing

(24) Jackson, P. F.; Johnson, B. F. G.; Lewis, J.; Mcpartlin, M.; Nelson, W. J. H. *J. Chem. Soc., Chem. Comm.* **1979**, 735.

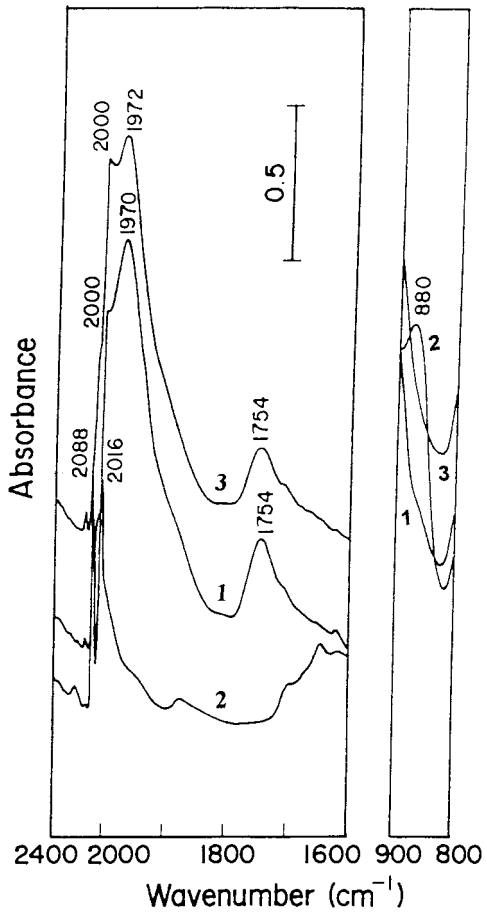

Figure 8. In situ FT-IR spectra characterization of the samples: (trace 1) synthetic sample c; (trace 2) oxidation fragmentation of sample c under O_2 of 100 Torr at 403 K for 2 h; (trace 3) reductive recarbonylation of oxidized sample under CO of 200 Torr and H_2 of 200 Torr atmosphere at 393 K for 12 h.

CO bands at 2088 and 2016 cm^{-1} (Figure 8, trace 2). At the same time, a low-frequency peak at 880 cm^{-1} is also present, which closely resembles that of Figure 4A, line 3. It is interesting that after exposure to CO + H_2 at 393 K for 12 h, the IR spectrum changed back to that observed prior to oxidation (Figure 8, trace 3). This process could be repeated several times.

Discussion

I. Confirmation of Ruthenium Carbonyl Clusters in Faujasite Cages. a. Sample a, $[Ru_3(CO)_{12}]/Na_{56}Y$. The Ru atoms form a triangle, with each ruthenium atom bearing four CO ligands, two in equatorial and two in axial positions (Figure 2B).[25] The $Ru(CO)_4$ units in this structure have local C_{2v} symmetry, whereas the overall $[Ru_3(CO)_{12}]$ cluster has D_{3h} symmetry.[25] CO ligands of such D_{3h} symmetry are expected to split to eight vibrational modes in the carbonyl stretching region, four of which are IR active, of symmetry species $1A''_2 + 3E'$ (Table 1).[26] This predicted number of bands is in agreement with the experimental carbonyl IR bands at 2060, 2030, 2019, and 2013 cm^{-1}, as shown in Figure 2A, trace 1, and Table 1.[27]

Comparing the assignment of carbonyl stretching bands of crystalline $[Ru_3(CO)_{12}]$ in hexane solution (Table 1), we identify the axial CO ligands of the $[Ru_3(CO)_{12}]$ guest in $Na_{56}Y$ at 2067s (axial E′) and 2025m cm^{-1} (axial A''_2). However, the equatorial CO ligands seem to be weakly IR active and probably constitute a shoulder on the string peak, in the expected region (2007−2015 cm^{-1}).[28] This is consistent with the inference that the diminishing of the contribution of the equatorial CO ligands to the IR bands may be due to the equatorial CO ligands interacting mainly with extraframework Na^+ cations and with possible Lewis acid sites (Al^{3+} ions) formed by the dehydration of $Na_{56}Y$. This interaction results in the shifting, broadening, and/or diminution of relative peak intensity. Moreover, there is a weak carbonyl stretching band (E′) at relatively high frequency, 2121 cm^{-1} for $[Ru_3(CO)_{12}]/Na_{56}Y$. This high-frequency peak for $[Ru_3(CO)_{12}]/Al_2O_3$ and for $[Ru_3(CO)_{12}]/SiO_2$, prepared by vapor impregnation in a vacuum, has also been found.[29] The wavenumber of this high-frequency peak increases, depending on the support, in the order SiO_2 (2110 cm^{-1}), $Na_{56}Y$ (2112 cm^{-1}), and Al_2O_3 (2134 cm^{-1}), which is also the order of relative activity of these materials.[28] This high-frequency IR band, which is not seen for $[Ru_3(CO)_{12}]$ in organic solution, is ascribed to the interaction of at least some of the $[Ru_3(CO)_{12}]$ with acid centers of the organic solution.[26]

b. Sample b, $[H_4Ru_4(CO)_{12}]/Na_{56}Y$. The cluster $[H_4Ru_4(CO)_{12}]$ has D_{2d} geometry, with the four ruthenium atoms forming a tetrahedron and with the four hydrogen atoms forming four edge-bridging hydrides.[30] The solution IR spectrum of this cluster shows intense bands at 2080 (axial), 2066, 2030, 2024, and 2009 cm^{-1} (equatorial) in the terminal carbonyl stretching region.[11] According to group theory, these five IR vibrational modes are assigned as symmetry species $2B_2 + 3E$, while the eleven Raman bands are assigned as symmetry species $2A_1 + B_1 + 2B_2 + 3E$ (Table 3).

The synthetic $[H_4Ru_4(CO)_{12}]$ in the cages shows terminal CO stretching bands at 2085 (axial), 2070, 2031, 2008, and 1992 cm^{-1} (equatorial) (Table 3). The stretching frequency of the equatorial CO bands is red-shifted by 17 cm^{-1} (2009 → 1992 cm^{-1}), while the axial CO bands blue-shifted by 5 cm^{-1} (2080 → 2085 cm^{-1}), referenced to those of $[H_4Ru_4(CO)_{12}]$ in hexane solution (Table 3). The characteristic shift of equatorial CO bands observed in $[H_4Ru_4(CO)_{12}]/Na_{56}Y$ is similar to those of metal carbonyls in solution containing Lewis acids such as $Al(C_2H_5)_3$, which have been examined extensively.[31] The equatorial terminal CO ligands are more basic than the axial terminal CO ligands,[32] which is borne out in the present pattern; the CO band shift is consistent with strong reaction of the oxygen in the equatorial terminal CO ligands of $[H_4Ru_4(CO)_{12}]$ primarily with extraframework Na^+ cations. Such a reaction is expected to result in a net electron withdrawal from the clusters, a decrease in back-bonding to the axial terminal CO ligands, a strengthening of the carbon−oxygen bond, and a shift of axial terminal CO bands to higher frequencies.

c. Sample c, $[Ru_6(CO)_{18}]^{2-}/Na_{56}X$. The structure of $[Ru_6(CO)_{18}]^{2-}$ is based on C_2 symmetry—three terminal CO ligands bound to each Ru atom of two out of six Ru atoms, two terminal CO ligands bound to each Ru atom of the other four Ru atoms, as well as two edge-bridging CO ligands, each bound to two Ru atoms, and two face-bridging CO ligands, each

(25) Tyler, D. R.; Levenson, R. A.; Gray, H. B. *J. Am. Chem. Soc.* **1978**, *100*, 7888.
(26) Quicksall, C. O.; Spiro, T. G. *Inorg. Chem.* **1968**, *7*, 2365.
(27) Battiston, G. A.; Bor, G.; Dietler, U. K.; Kettle, S. F. A.; Rossetti, R.; Sbrignadello, G.; Stanghellini, P. L. *Inorg. Chem.* **1980**, *19*, 1961.
(28) Goodwin, J. G., Jr.; Naccache, C. *J. Mol. Catal.* **1982**, *14*, 259.
(29) Melson, G. Presented at the Spring Symposium of the Pittsburgh Catalysis Society, Monroeville, PA, May 28−30, 1980.
(30) Wilson, R. D.; Wu, S. M.; Love, R. A.; Bau, R. *Inorg. Chem.* **1978**, *17*, 1271.
(31) Shriver, D. F. *J. Organomet. Chem.* **1975**, *94*, 259.
(32) Lamb, H. H.; Gates, B. C.; Knozinger, H. *Angew. Chem., Int. Ed. Engl.* **1988**, *27*, 1127.

bound to three Ru atoms (Figure 4C).[20b,20c] Group theory, therefore, predicts 18 CO stretching modes (11A + 7B), four of which are IR-active. The predicted number of bands were observed either in solution (2006s, 1986vs, 1930m, and 1754w cm^{-1}) or in $Na_{56}X$ cages (2000s, 1972vs, 1925m, and 1747w cm^{-1}), as summarized in Table 4. However, the stretching frequencies (1747 cm^{-1}) of the CO ligands in $[Ru_6(CO)_{18}]^{2-}/Na_{56}X$ are shifted to lower energy by approximately 7 cm^{-1} compared to that of $[Ru_6(CO)_{18}]^{2-}$ (1757 cm^{-1}) in CH_2Cl_2 solution. This shift is consistent with the formation of ion pairs with extraframework Na^+ cations. In contrast to previous results,[10,17a] the terminal CO bands unexpectedly shifted to lower frequency. A tentative explanation is that under the synthesis conditions, almost all the water is removed, as evidenced by the IR spectrum (Figure 4A, trace 4). Presumably, most of the $Na_{56}X$ cage cations are not hydrated and behave as Lewis acids, interacting with not only the more strongly basic bridging CO ligands but also the less basic terminal CO ligands of the ruthenium cluster dianion.

II. Details of the Anchoring Site of Ruthenium Carbonyl Guest inside Faujasite Cages. One of the main issues complicating the synthesis and characterization of metal clusters in faujasite is the possible simultaneous formation of metal clusters or crystallites on the outside of faujasite. However, the results of the work here suggest that virtually all the ruthenium carbonyl clusters were formed and confined to faujasite cages. Extraction of the organometallic species from synthetic samples by hexane or CH_2Cl_2 solution was unsuccessful. The results are consistent with a "ship-in-a-bottle" synthesis of the ruthenium carbonyl clusters: the precursor $[Ru^{III}(NH_3)_6]$ or $[Ru_3(CO)_{12}]$ is presumed only to be located inside the α-cages by its molecular size under ion exchange or vapor dispersion preparation. The synthetic $[H_4Ru_4(CO)_{12}]$, $[Ru_6(CO)_{18}]^{2-}$, or $[HRu_6(CO)_{18}]^-$ clusters are small enough to fit in the α-cages of $Na_{56}X$ but are too large to match the *β*-cage and hexagonal prisms and to diffuse through the apertures. No IR band shifts between crystalline Ru carbonyl clusters and their site of deposition onto the extrafaujasite were observed. Therefore, present IR band shifts imply that the $[Ru_3(CO)_{12}]$, $[H_4Ru_4(CO)_{12}]$, $[Ru_6(CO)_{18}]^{2-}$, or $[HRu_6(CO)_{18}]^-$ guests should be encapsulated in the α-cages. Assuming the formation of $[Ru_6(CO)_{18}]^{2-}$ guest on the extrfaujasite, the reversible reformation of $[Ru_6(CO)_{18}]^{2-}$ resulting from CO and H_2 chemisorption on its oxidation state will be unsuccessful, since extrafaujasite Ru clusters coalescence under severe reductive regeneration conditions.

X-ray diffraction[33] and neutron diffraction measurements[34] have established that approximately 55% of the extraframework Na^+ cations in dehydrated faujasite are located inside the α-cages at site II, around 30% in the *β*-cages at site I′, 7−8% at site I at hexagonal prisms, with the remainder at site III (Figure 1). Jelinek et al.[35] provided insight into the interactions between the extraframework Na^+ cations and the adsorbed guest molecules using ^{23}Na MAS NMR spectra. Introduction of metal carbonyl guest into the cavities of faujasite causes a downfield shift of the ^{23}Na signal, ascribed to the site II Na^+ cations. No appreciable band shifts of the ^{23}Na signal were observed, ascribed to the site I′ and site I Na^+ cations (Figure 1). These observations, together with our IR band shifts of the guest filling in faujasite cages, lead one to propose that a strong anchoring

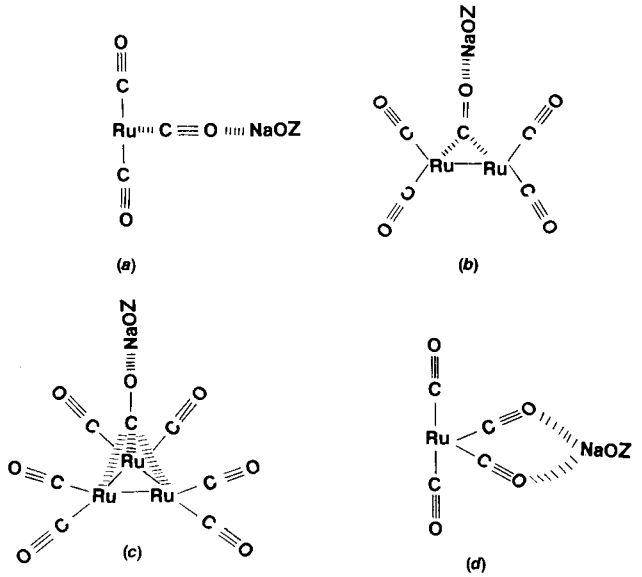

Figure 9. Model a shows possible anchoring of mononuclear carbonyl site for the α-cage-located $[H_4Ru_4(CO)_{12}]$ guest. Model b shows possible anchoring site of edge-bridging CO ligands bound to two Ru atoms for the α-cage-located $[Ru_6(CO)_{18}]^{2-}$ guest. Model c shows possible anchoring site of face-bridging CO ligands bound to three Ru atoms for the α-cage-located $[Ru_6(CO)_{18}]^{2-}$ guest. Model d shows possible anchoring of mononuclear carbonyl sites for the α-cage-located $[Ru_3(CO)_{12}]$ guest.

interaction occurs between the guest and the Na^+ cations at site II in the α-cage through involvement of the oxygen end of the bridging or equatorial terminal carbonyl ligands, thereby reducing the anchoring site geometry in comparison with that of the free guest molecules. For $[Ru_4H_4(CO)_{12}]/Na_{56}Y$, the equatorial CO ligands show a red shift in the IR spectrum. One can infer that the steric and volume filling requirements of the encapsulated $[Ru_4H_4(CO)_{12}]$ in the α-cage favor the four *trans*-ZONa···(OC)Ru structure (where CO is IR-active equatorial CO), having distorted D_{2d} symmetry involving four Na^+ site II cations (there are four Na^+ site II cations per α-cage in Figure 1). One of four structures is depicted in Figure 9a.

The $Na_{56}X$ anchoring of $[Ru_6(CO)_{18}]^{2-}$ model is shown in Figure 9 parts b and c. The basicity of the oxygen in the CO ligands of metal clusters depends on the CO coordination geometry.[32] Triply bridging CO ligands are more basic than doubly bridging CO ligands, which are significantly more basic than terminal CO ligands. This provided supporting evidence for the present model—the oxygen end of two triply bridging CO ligands reacts with the two extraframework Na^+ α-cage cations, and the oxygen end of two doubly bridging CO ligands reacts with the two other extraframework Na^+ α-cage cations. These are two ZONa···(μ_3-OC)Ru_3 and two Ru_2(μ_2-CO)··· NaOZ skeletons involving four Na^+ site II cations (Figure 9 parts b and c).

The binding site model of $[Ru_3(CO)_{12}]/Na_{56}Y$ is preferred for the interaction of the oxygen end of two cis carbonyl ligands bound to a Ru atom, with a single extraframework Na^+ α-cage cation. One of three *cis*-ZONa···$(OC)_2$Ru is illustrated in Figure 9d (where CO is IR-active equatorial CO). This model is also consistent with the inference of a decrease in $[Ru_3(CO)_{12}]$ D_{3h} symmetry in its intrafaujasite anchoring state.

III. Mechanism of Ruthenium Carbonyl Clusters Formation in Faujasite Cages. a. $[Ru(NH_3)_6]^{3+}$ Reductive Carbonylation in $Na_{56}X$ Cages. Hexammineruthenium(III) in the $Na_{56}X$ zeolite is very unstable under a CO and H_2 atmosphere. As shown in Figure 4A, trace 2, on raising the temperature to

(33) Eulenberger, G. R.; Shoemaker, D. P.; Keil, J. G. *J. Phys. Chem.* **1967**, *71*, 1812.
(34) Fitch, A. N.; Jobic, H.; Renouprez, A. *J. Phys. Chem.* **1986**, *90*, 1311.
(35) Jelinek, P. Ph.D. Thesis, Department of Chemistry, University of Toronto, 1993.

353 K, a major carbonyl stretching vibration at 1939 cm^{-1} appears, which can be assigned to $[Ru(NH_3)_5(CO)]^{2+}$ in $Na_{56}X$.[17b,22] The band at 1468 cm^{-1} indicates that some of the NH_3 ligands are released from the coordination sphere of the complex, forming NH_4^+ ions,[16] while the intensity of the 1640 and 1356 cm^{-1} bands due to NH_3 ligands decreased.[17] This change in the IR spectrum of the N−H vibrations is typical upon reduction of Ru^{III} in faujasite.[28] The diffuse reflectance spectrum at 390 and 280 nm also showed the presence of an $[Ru(NH_3)_5(CO)]^{2+}$ intermediate (Figure 5, trace 2). This ligand conversion is depicted in eq 1:

$$2[Ru(NH_3)_6]^{3+} + 2CO + H_2 \xrightarrow{353\ K} 2[Ru(NH_3)_5(CO)]^{2+} + 2NH_4^+ \quad (1)$$

When the temperature reached 393 K for 30 min, the CO band (1393 cm^{-1}) of $[Ru(NH_3)_5(CO)]^{2+}$ disappeared and two doublet carbonyl bands emerged at 2088 and 2014 and 2048 and 1952 cm^{-1}, which are attributed to bicarbonylruthenium(I) and tricarbonylruthenium(I) in $Na_{56}X$, respectively.[17b,22] The formation of $[Ru^I(CO)_2]$ and $[Ru^I(CO)_3]$ would be proposed as eqs 2 and 3,

$$2[Ru(CO)]^{2+} + 2CO + H_2 \xrightarrow{393\ K,\ 30\ min} 2[Ru(CO)_2]^+ + 2H^+ \quad (2)$$

$$2[Ru(CO)]^{2+} + 4CO + H_2 \xrightarrow{393\ K,\ 30\ min} 2[Ru(CO)_3]^+ + 2H^+ \quad (3)$$

It is noteworthy that the IR spectrum of the ruthenium carbonyl intermediate shows a low-frequency band at 862 cm^{-1}, which is ascribed to the adduct of the mononuclear ruthenium carbonyl species with the oxygen of the $Na_{56}X$ framework, either $(CO)_2Ru^I-O-Al(Si)$ or $(CO)_3Ru^I-O-Al(Si)$. Bicarbonylruthenium(I) and tricarbonylruthenium(I) are converted into dianionic ruthenium carbonyl clusters after 22 h at 393 K, while the lower frequency 862 cm^{-1} band disappears. This conversion is represented in eqs 4 and 5,

$$6[Ru(CO)_2]^+ + 6CO + 4H_2 \xrightarrow{393\ K,\ 22\ h} [Ru_6(CO)_{18}]^{2-} + 8H^+ \quad (4)$$

$$6[Ru(CO)_3] + 4H_2 \xrightarrow{393\ K,\ 22\ h} [Ru_6(CO)_{18}]^{2-} + 8H^+ \quad (5)$$

Protons are produced during these reductive processes, attaching to the lattice oxygen of faujasite framework and forming an OH group inside the α-cage, which is detected by an IR peak at 3654 cm^{-1} (not shown).

The reflectance UV−vis spectrum is in good agreement with the IR results, giving two absorption bands at 235 and 287 nm (Figure 5, trace 4), practically identical to that of $[PPN]_2[Ru_6(CO)_{18}]^{2-}$ in THF solution (235, 285 nm in Table 2). EXAFS analysis also confirms the final formation of $[Ru_6(CO)_{18}]^{2-}$ in $Na_{56}X$.

As shown in Figure 8, trace 2, $[Ru_6(CO)_{18}]^{2-}$ is fragmented into mononuclear ruthenium species under an O_2 atmophere, exhibiting CO bands at 2088 and 2016 cm^{-1}, the same as those of $[Ru^I(CO)_2]/Na_{56}X$ described in Figure 4, trace 3. Simultaneously, the low-frequency peak at 880 cm^{-1} appears, closely resembling the peak at 862 cm^{-1} in Figure 4, trace 3, which was ascribed to $(CO)_2Ru^I-O-Al(Si)$. However, the 18 cm^{-1} blue shift here is probably associated with the variation of the water concentration in $Na_{56}X$.[36] $(CO)_2Ru^I-O-Al(Si)$ was recarbonylated under a CO and H_2 atmosphere at 393 K. The IR bands at 2088, 2000, 1972, and 1754 cm^{-1} of the resultant sample (Figure 8, trace 3) are practically identical to those of $[Ru_6(CO)_{18}]^{2-}/Na_{56}X$ (Figure 8, trace 1), by comparison of wavenumber value, intensity, the full width at half-maximum (fwhm) of CO bands, and the constant intensity ratio of the CO_t/CO_b bands between the intial $[Ru_6(CO)_{18}]^{2-}/Na_{56}X$ and recarbonylated sample. This indicates that $[Ru_6(CO)_{18}]^{2-}$ was reformed inside the α-cages. The recarbonylated sample became pale yellow again (λ_{max} = 235 and 287 nm in the UV−vis spectrum). The process was carried out several times without any significant change in the spectrum of the carbonylated form. Therefore, we conclude that the oxidation fragmentation and reductive regeneration are reversible under these conditions. The facile rearrangments of the ruthenium carbonyl species in the $Na_{56}X$ α-cages are evidence of their mobility in the $Na_{56}X$, corresponding to their solution-like behavior.[37] Similar chemistry has been observed for decarbonylated Ru−Co carbonyl clusters on $Na_{56}Y$.[17a] This reversible processes is illustrated in eq 6,

$$[Ru_6(CO)_{18}]^{2-} \underset{CO + H_2,\ 393\ K}{\overset{O_2,\ 403\ K}{\rightleftharpoons}} 6[Ru^I(CO)_2] + 6CO \quad (6)$$

b. Formation of $[Ru_4H_4(CO)_{12}]/Na_{56}Y$. Treatment of $[Ru_3(CO)_{12}]$ with H_2 gives $[Ru_4H_4(CO)_{12}]$, conveniently in high yield and purity. Excellent analytical data were obtained for our product, which displays five maxima in the carbonyl stretching region of the IR spectrum (Figure 3A, trace 2, and Table 3). The CO/Ru stoichiometry of about 3 mol of evolved CO to 1 mol of supported $[Ru_3(CO)_{12}]$ (where the stoichiometry is derived from detection by gas chromatography) is consistent with the surface reaction

$$4[Ru_3(CO)_{12}] + 6H_2 \xrightarrow{363\ K} 3[Ru_4H_4(CO)_{12}] + 12CO \quad (7)$$

$$CO/Ru_3 \text{ molar ratio} = 3$$

involving the nucleation of the starting Ru_3 cluster into the Ru_4 hydrido species.

As expected, $Na_{56}Y$ encapsulated $[Ru_3(CO)_{12}]$ demonstrates fair activity, being converted to $[Ru_4H_4(CO)_{12}]$ in a hydrogen atmosphere at 363 K. Higher reaction temperature should, however, be avoided, since $[Ru_4H_4(CO)_{12}]$ starts to decompose to metallic Ru above 383 K. Knox et al.[38] showed that $[Os_3(CO)_{12}]$ in octane solution at 393 K, under hydrogenation, formed $[Os_3H_2(CO)_{10}]$ as the first step. $[Os_4H_4(CO)_{12}]$ was subsequently obtained by additional treatment of the trinuclear hydride cluster with H_2. A remarkable peculiarity of the $Na_{56}Y$ internal surface-mediated route is that $[Ru_3H_2(CO)_{10}]$ does not seem to be formed as a stable intermediate in the α-cages, as suggested by our IR spectrum. The unstable $[Ru_3H_2(CO)_{10}]$ quickly reacted with H_2 at 363 K to form $[Ru_4H_4(CO)_{12}]$. Such $[Ru_3(CO)_{12}]$ is much more reactive than the Os homologue, corresponding to their solution-like behavior.[38]

In addition, a mechanism of $[Ru_4H_4(CO)_{12}]$ formation involving surface OH groups of the α-cages cannot be ruled out. However, this reactivity, leading to the formation of the grafted surface species $HM_3(CO)_{10}(OSi\equiv)$, is possible only in the

(36) Liu, A.-M.; Shido, T.; Ichikawa, M. *J. Chem. Soc., Chem. Commun.*, in press.
(37) (a) Chini, P.; Martinengo, S. *Inorg. Chim. Acta*. **1969**, *3*, 21. (b) Chini, P.; Martinengo, S. *Inorg. Chem. Acta*. **1969**, *3*, 315.
(38) Knox, S. A. R.; Koepke, J. W.; Andrews, M. A.; Kaesz, H. D. *J. Am. Chem. Soc*. **1975**, *97*, 3942.

absence of hydrogen, by the oxidative addition of a silanol group into a metal−metal bond of the cluster frame.[39] The surface OH group chemisorbed cluster does not transform into $[H_4M_4(CO)_{12}]$ if subsequently heated in a hydrogen atmosphere. Consequently, in the reported synthesis of $[H_4M_4(CO)_{12}]$ inside the α-cages, it is very important to avoid any chemical interaction of the cluster precursor with the −OH group of the framework.

IV. Role of Topology of Faujasite in the Selective Formation of Ruthenium Carbonyl Clusters. Faujasite-type zeolites X and Y are synthetic materials with framework structures topologically related to the natural mineral faujasite. The unit cells are cubic and built from 192 corner-sharing SiO_4^{4-} and AlO_4^{5-} tetrahedra. Differences between X and Y stem from variations in the Si/Al ratio. These aluminosilicates are usually synthesized in Na-bearing systems and have compositions $Na_xAl_xSiO_{192-x}O_{384}$ ZH_2O, where x ranges from 96 to 74 for faujasite X and from 74 to 48 for faujasite Y, while Z drops from 270 to 250 as x decreases.[5,6] The aluminosilicates are built up of β-cages linked by hexagonal prisms (or doublet-six rings). The large cages (α-cages) thus formed possess an internal diameter of ca. 13 Å and are accessible (and interconnected) through four windows (12-membered rings) with a diameter of ca. 7.4 Å (Figure 1). These large openings allow penetration of metal carbonyls and organometallic molecules, although diffusion, particularly at low temperature, may be sluggish. In the present sample a, the D_{3h} $[Ru_3(CO)_{12}]$ guest has a kinetic magnitude in the range 6.6 Å × 7.4 Å × 8.1 Å[40] and, therefore, hardly gains free access to the α-cages though the entrance pore of faujasite. Thermal treatment at 333 K results in the possible entrance of the $[Ru_3(CO)_{12}]$ guest into the α-cages, apparently as a consequence of the vaporization re-formation geometry of the $[Ru_3(CO)_{12}]$ guest.

A wide range of chemical composition, a well-defined crystal structure, a high interface area, uniformity of interface, a high internal electric field, high CO gas accessibility, and good thermal stability (up to about 1000 K) are properties of faujasite,[7,41,42] as compared to more classical supports (e.g., silica gels and active alumines). This makes faujasite a versatile material for use as an inorganic support and interface adduct. For example, the oxide framework of faujasite is considered to be a macrospheroidal, multisite, multidentate "zeolate" ligand.[1] This framework favors the synthesis of organometallic compounds such as the present synthetic $[Ru_6(CO)_{18}]^{2-}/Na_{56}X$, $[H_4Ru_4(CO)_{12}]/Na_{56}Y$, and $[HRu_6(CO)_{18}]^-/Na_{56}Y$.

In contrast, the IR spectrum of silica-supported sample e showed terminal bands at 2072 and 2045 cm^{-1} but no bridging CO band. These IR peaks are an indication of CO adsorbed on metallic Ru particles of sample e.[43] Neither $[Ru_6(CO)_{18}]^{2-}$ nor $[HRu_6(CO)_{18}]^-$ was formed. In addition, the $[PPN]_2[Ru_6(CO)_{18}]$ was impregnated onto silica, which showed instability and produced additional chemical species. The IR spectrum of these unassigned chemical species showed bands at 2122, 2035, and 1950 cm^{-1}, fundamentally different from the spectrum of the original $[PPN]_2[Ru_6(CO)_{18}]$ clusters, suggesting that $[Ru_6(CO)_{18}]^{2-}$ broke down on the silica surface. The results are therefore consistent with the hypothesis that the internal topology of the α-cages plays a significant role in the stabilization and consequently in the selective formation of ruthenium carbonyl clusters.

Brönsted acidity of faujasite is correlated with OH bond strength, which can be directly monitored by the corresponding IR stretching frequency at 3745 cm^{-1} (occurring at the exterior), at 3660 cm^{-1} (occurring inside the α-cage (bridged hydroxyls)), and at 3556 cm^{-1} (occurring at small cavities of faujasite).[44] Brönsted acidic strength of the bridging OH groups in the α-cages increases with the increasing Si/Al ratio due to enhanced electronegativity of the faujasite framework. Faujasite Y is therefore more acidic than faujasite X. It has been reported that the α-cages of $Na_{56}X$ are sufficiently basic to provide an efficient medium for the synthesis of anionic metal carbonyl clusters.[45] The chemistry of anionic metal carbonyl clusters in $Na_{56}X$ cages parallels its chemistry in basic solutions or in basic metal oxides. The formation of neutral/monoanionic metal carbonyl clusters in $Na_{56}Y$ cages is similar to that occurring in a Lewis base solution.[46] These patterns are borne out in the present results—the neutral $[Ru_3(CO)_{12}]$, $[H_4Ru_4(CO)_{12}]$, and monoanionic $[HRu_6(CO)_{18}]^-$ were synthesized inside $Na_{56}Y$ α-cages, whereas dianionic $[Ru_6(CO)_{18}]^{2-}$ was synthesized inside $Na_{56}X$ α-cages. Eady et al.[20a] reported that addition of excess sulfuric acid to the initial tetrahydrofuran of $[Ru_6(CO)_{18}]^{2-}$ yields $[HRu_6(CO)_{18}]^-$. It is therefore considered that dianionic $[Ru_6(CO)_{18}]^{2-}$ would be oxidized to monoanionic $[HRu_6(CO)_{18}]^-$ by Brönsted acid and Lewis acid sites (Na^+ and Al^{3+}) of $Na_{56}Y$, as occurs with oxidizing agents.[47] These results also give an indication of the possibilities for modification of the reactivity in the solventlike cages of the zeolite by changing the Si-to-Al ratio.

Conclusions

$[Ru_3(CO)_{12}]$ guests in $Na_{56}Y$ were thermally activated from 298 to 363 K, in a hydrogen atmosphere, generating intrafaujasite anchoring of $[H_4Ru_4(CO)_{12}]$. $[Ru(NH_3)_6]^{3+}$ in $Na_{56}X$ was thermally activated progressively from 298 to 393 K, in an atmosphere of CO and H_2. The generation proceeded through conversion of the intermediates $[Ru(NH_3)_5(CO)]^{2+}$ and $Ru^I(CO)_3$ to $[Ru_6(CO)_{18}]^{2-}$. The characterization of the structure and properties of the samples used a multianalytical approach based on FT-IR, UV−vis and PXRD spectroscopies, $^{13}CO/^{12}CO$ isotopic exchange reaction, oxidation fragmentation, and reductive regeneration. The Na^+ cations and topology of faujasite, it was suggestd, play a significant role in the anchoring and selective formation of ruthenium carbonyl clusters.

These multianalytical methods will motivate both new and established scientists to study further the analogue with other types of zeolite (such as ZSM-5 or MCM-41) anchoring of metal carbonyl clusters. Faujasite-mediated synthesis of metal carbonyl clusters can provide routes to compounds not accessible through conventional solution techniques. Further, higher yield clusters, as well as a better understanding of the nucleation process of cluster formation and of the resulting chemical properties, can be expected. We predict that this research is of interest to the inorganic and organometallic chemistry and catalysis communities.

IC9709990

(39) Zanderighi, G. M.; Dossi, C.; Ugo, R.; Psaro, R.; Theolier, A.; Choplin, A.; D'Ornelas, L.; Basset, J. M. *J. Organomet. Chem.* **1985**, *296*, 127.
(40) Battiston, G. A.; Bor, G.; Dietler, U. K.; Kettle, S. F. A.; Rossetti, R.; Sbrignadello, G.; Stanghellini, P. L. *Inorg. Chem.* **1980**, *19*, 1961.
(41) Preuss, E.; Linden, G.; Peuckert, M. *J. Phys. Chem.* **1985**, *89*, 2955.
(42) Mortier, W. J.; Schoonheydt, R. A. *Prog. Solid State Chem.* **1985**, *16*, 1.
(43) Yokomizo, G. H.; Louis, C.; Bell, A. T. *J. Catal.* **1989**, *120*, 1.
(44) Jacobs, P. A.; Mortier, W. J. *Zeolites* **1982**, *2*, 226.
(45) (a) Schneider, R. L.; Howe, R. F.; Watters, K. L. *Inorg. Chem.* **1984**, *23*, 4600. (b) Connaway, M. C.; Hanson, B. E. *Inorg. Chem.* **1986**, *25*, 1445.
(46) Pierantozzi, R.; Valagene, E. G.; Nordquist, A. F.; Dyer, P. N. *J. Mol. Catal.* **1983**, *21*, 189.
(47) (a) Albano, V.; Chini, P.; Scatturin, V. *Chem. Commun.* **1968**, 163. (b) Chini, P. *Chem. Commun.* **1967**, 440.